Jour. Petrol. Soc. Korea
Vol. 5, No. 2, p. 161~167, 1996

Diopside CSD (crystal size distribution) in the Contact Metamorphic Aureole (Hwanggangni Formation) near the Daeyasan Granite Goesan, Korea

Sangmyung Kim and Hyung Shik Kim

Department of Earth and Environmental Sciences, College of Sciences, Korea University, 5-1 Anam-dong, Sungbuk-ku, Seoul 136-701, Korea

ABSTRACT : The CSD (crystal size distribution) of diopside crystals in the calc-silicate hornfels of the Hwanggangni Formation intruded by the Cretaceous Daeyasan granite shows the patterns of continuous nucleation and growth. There is correlation between the distance from the intrusion contact and the slopes from the linear part of log(population density) vs. size diagrams. In the log(population density) vs. size diagrams of the samples systematically collected from the intrusion contact, two different groups are recognized; the slopes for the samples near the intrusion contact (horizontal distance from the contact less than 50 m) are gentler (1500 cm^{-1}) than those for the samples away from the intrusion contact (2500 cm^{-1}, distance from the contact greater than 100 m). These differences may reflect the differences in growth rates and crystallization time, or the differences in diopside-forming reactions. All of the log(population density) vs. size diagrams show depletion of smaller crystals. The observed depletion may be due to Ostwald ripening or the changes in nucleation rates as the reactant phases diminishes. Similar grouping is also possible for the observed degree of depletion of smaller crystals; the depletion decreases with increasing distance from the intrusion contact, suggesting temperature-dependent rates of Ostwald ripening.

Key words : CSD, diopside, nucleation, crystal growth, Ostwald ripening

Introduction

The crystal size distribution (CSD) of rocks, like other textural features, reflects the time-integrated rate of processes experienced by the rocks. Three processes of CSD in crystalline rocks free from deformation throughout the history of the rocks include; (1) nucleation, (2) crystal growth and (3) Ostwald ripening (a surface-energy driven coarsening process or a process similar to grain growth in metallurgy). Because of the time-integrated nature of processes, it is practically impossible to decode or interpret the observed CSD patterns quantitatively. The CSD theory, originally developed by chemical engineers (Randolph and Larson, 1971), however, makes it possible to obtain useful kinetic parameters such as nucleation and growth rates from the observed CSD patterns without resort to the complex theories on kinetics. The CSD theory is based on population balance of MSMPR (Mixed Suspension, Mixed Product, and Removal) system that is conceptually similar to an open magma chamber. The theory has been applied to both igneous and metamorphic rocks by Cashman and Marsh (1988), Cashman and Ferry (1988), Marsh (1988), and Cashman (1991).

In this study, the CSD theory has been applied to diopside crystals in calc-silicate hornfels to infer the characteristics of the three processes-nucleation, growth and Ostwald ripening. We have chosen a contact aureole because it is an ideal place to test the correlation between kinetic processes and temperature conditions.

Geological setting

The study area is composed of the Hwanggangni formation and the Cretaceous Daeyasan granite. The Hwanggangni formation was previously composed of pebble bearing phyllite before intrusion of the Daeyasan granite. Calcsilicate hornfels (Hwanggangni Formation) was formed by the intrusion of the Cretaceous Daeyasan granite (Fig. 1). The age and depth of intrusion are 110 Ma and 1.5~5 km, respectively (Jin *et al.*, 1993). The contact aureole is characterized by the wollastonite, diopside, and tremolite zones (Kim and Kim, 1996). The mineral assemblages in the tremolite zone are tremolite, calcite, quartz, K-feldspar, phlogopite and clinozoisite. Calcsilicate hornfels in the diopside zone mainly consists of diopside, quartz, grossular, and vesuvianite. The mineral assemblages in the wollastonite zone are wollastonite, phlogopite, diopside and grossular. Quartz and calcite pebbles are omnipresent in this aureole. According to previous study (Kim and Kim, 1996), a possible upper limiting value of X_{CO_2} of diopside zone is 0.2 or 0.02 which corresponds to the temperature 400℃ to 460℃ at 1 kbar or 350℃ to 430℃ at 0.5 kbar, respectively. The sampling sites are located in the wollastonite and diopside zones (Fig. 1).

In the hornfelsic lithology, no unambiguous evidence for deformation such as subgrain boundary or mechanical twin have been found, so we do not considered effect of deformation after intrusion.

CSD theory

The CSD theory discussed below is brief, and further details can be found in Marsh (1988).

The key equation of the CSD theory is

$$n = n_0 \exp(-L/G\tau) \quad (1)$$

$$\text{or } \ln(n) = \ln(n_0) - L/G\tau \quad (2)$$

where n_0, G, τ, n, and L represent nucleation density, growth rate, time for crystallization (or residence time), number of crystals (or population density), and size of crystals respectively. Equations (1) or (2) is the analytical solution of the equation;

$$\frac{dn}{dl} + \frac{n}{G\tau} = 0 \quad (3)$$

which represents balancing of populations for a size interval.

The shape of frequency diagram depends on size interval. Hence as size interval decreases, the distribution function converges to zero. These problems can be solved by considering cumulative frequency which is the total number of crystals of size L and number of smaller crystals per unit volume;

$$N(L) = \int_0^L n(L)\, dL \quad (4)$$

where n(L) is the size distribution function or

$$n(L) = \frac{dN(L)}{dL} \quad (5)$$

The log n(L) vs. size(L) diagram is used to extract parameters such as n_0 and $G\tau$ in equation (2).

Methods and Procedures

Seven samples of calc-silicate hornfelses were collected to measure the size of diopside crystals from the contact aureole. These samples were systematically collected from the intrusion contact to the margin of the diopside zone (along the stream in the boxed region of Fig. 1). Thin sections were prepared with its thickness ~20 μm so that the interference color of diopside crystals is straw yellow whereas that of quartz and vesuvianite is dark gray. This procedure makes it easier to distinguish diopside crystals from quartz and vesuvianite in digital images. Digital images of the samples were taken from a microscope using a video camera connected to a Macintosh computer. Ten images were taken from each field

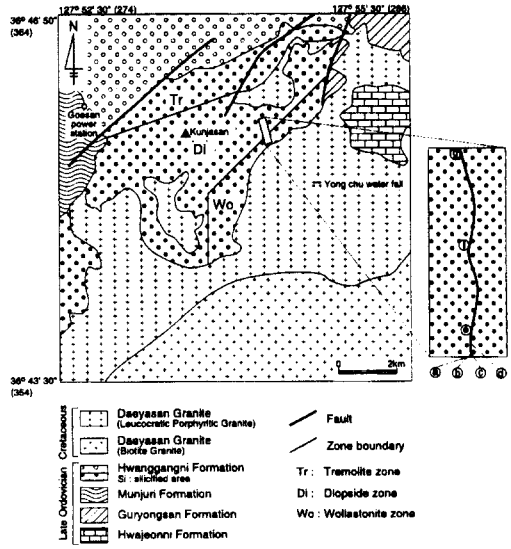

Fig. 1. Geological map of the study area (Goesan, Korea). Sampling sites are in the boxed area.

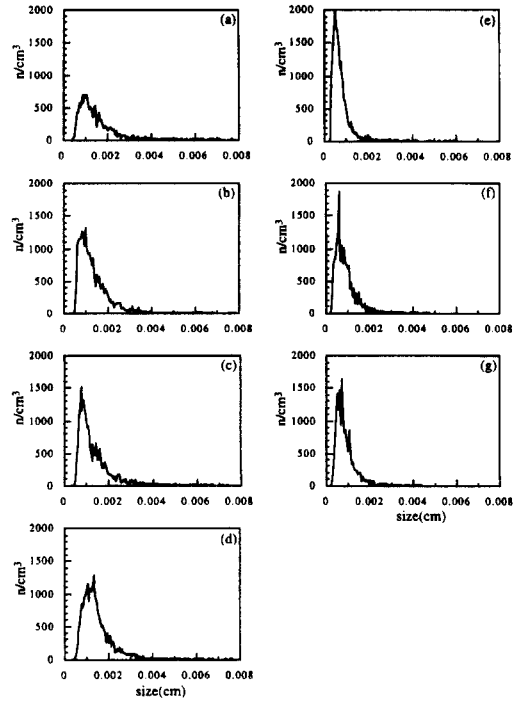

Fig. 2. Frequency diagrams of diopside crystals. The sampling sites for each sample are shown in Fig. 1 and Table 1.

of view; one is a plane-polarized-light image and the others are crossed-polarized-light images taken while rotating both polarizer and analyzer by 10°. This procedure facilitate the identification of neighboring diopside crystals or the grain boundaries. Grain boundaries were traced on plane-polarized-light images and the traced grain boundaries were scanned by NIH Image (Rasband, 1994). Finally, the major axis of best fitting ellipse for each grain was measured using the built-in function of the NIH Image program.

Since the crystal size was measured from two dimensional images, we have converted two dimensional measurement into three dimensional data using the empirical equation;

$$N_v = (N_a)^{1.5} \quad (6)$$

Where N_v and N_a stand for number of crystals per unit volume and unit area, respectively (Cashman and Ferry, 1988).

Results

The obtained size data from seven samples are shown in Figs. 2, 3, and 4. The diopside crystals of the samples collected within 50 meters from the intrusion contact (Fig. 2a, b, c, and d) show broader distribution of crystal size than those of the samples farther away from the intrusion contact. The diagrams also show the enrichment of smaller crystals in the samples more than 50m from the intrusion contact.

In order to obtain population density of diopside crystals, cumulative frequency diagrams were constructed (Fig. 3). The shapes of the cumulative frequency curves in Fig. 3 is characterized by sigmoidal shape in the smaller crystals. The sigmoidal shape in the diagrams represents larger increase for the crystals of intermediate size ($0.0005<L<0.002$cm in Fig. 3a), and smaller increase for the crystals belonging to size interval less than 0.0005cm and more than 0.002cm in Fig 3a. The size distribution function n(L) is calculated by using the equation (5). The size vs. ln(n(L)) (log po-

pulation density or ln(n) hereafter) diagrams are shown in Fig. 4. Kinetic information, such as the nucleation density n_0, reciprocal of the rates of crystal growth (G) multiplied by time (τ) for crystallization can be calculated by equation (2) from Fig. 4. The calculated kinetic parameters from equation (2) and Fig. 4 are summarized in Table 1.

From these observations, the general features of the diopside CSD can be made; (1) The slope of ln(n) vs. size diagrams increases with increasing distance. The slopes in the samples within 50m from the contact are nearly identical but different from those for the samples of more than 100 m. The difference is

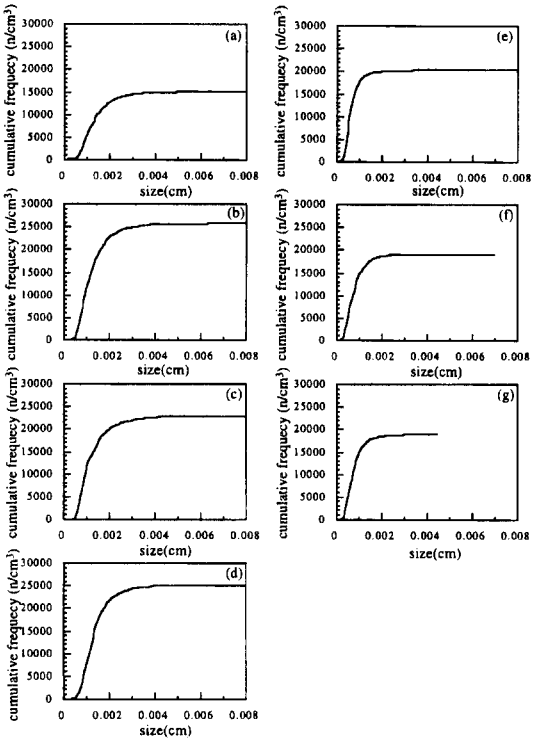

Fig. 3. Cumulative frequency diagrams of diopside crystals.

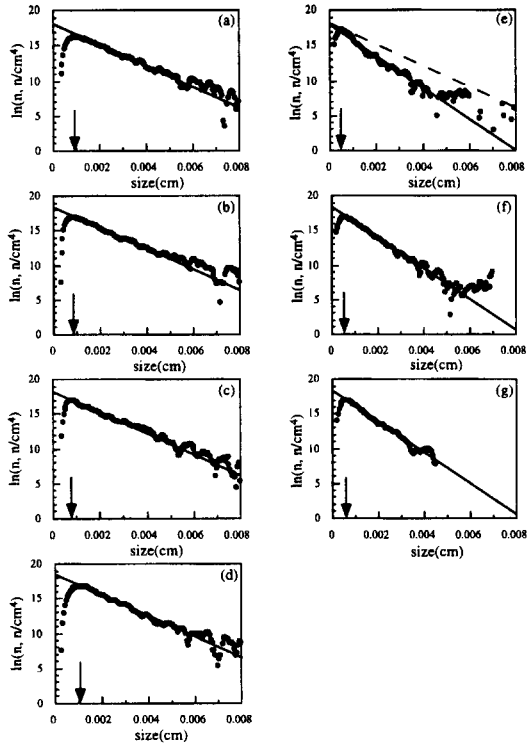

Fig. 4. ln(n) vs. size diagrams for each samples. Arrows indicate critical size (Lc) at which depletion of smaller crystals is observed. The dashed line in diagrams for (e) denotes the slope of samples near the intrusion contact (<50 m, (a), (b), (c), and (d)). The deviation from linear distribution in size classes > 0.004 cm is due to the error during differentiation of cumulative frequency diagrams.

Table 1. Kinetic parameters calculated from ln(n) vs. size diagrams.

Sample	Horizontal distance from the contact	$1/G\tau$, n_0	L_c	sheet name	national grid
(a)	5 m	1500 cm^{-1}, 3269017/cm^4	0.001 cm	Sogri	360.7/280.5
(b)	10 m	1500 cm^{-1}, 3269017/cm^4	0.001 cm		
(c)	15 m	1500 cm^{-1}, 3269017/cm^4	0.001 cm		
(d)	40 m	1500 cm^{-1}, 3269017/cm^4	0.001 cm		
(e)	120 m	2500 cm^{-1}, 3269017/cm^4	0.0005 cm		
(f)	461 m	2500 cm^{-1}, 3269017/cm^4	0.0005 cm		
(g)	861 m	2500 cm^{-1}, 3269017/cm^4	0.0005 cm		361.1/279.7

shown in Fig. 4 (e) in which both its own slope and the slope for samples near intrusion contact (dashed line) are drawn. (2) Arrows in Fig. 4 indicating the critical size (L_c) at which depletion of smaller crystals is observed, decreases with increasing distance from the intrusion contact.

Discussion

The two different groups of the diopside CSD patterns in the study area have been discussed with the distance from the intrusion contact. The distance from the intrusion contact mentioned so far is the measure on the basis of geological map. Thus vertical granite to country rock contact is implicitly assumed. In the study area, however, there is a possibility that the intrusion contact is not vertical as described by Hong (1985). Hong (1985) suggested a gently dipping intrusion contact based on the observations of intermittent exposures of the granite along the stream of Fig. 1. The true distance from the contact can be reduced depending on the dipping angle of the intrusion contact. For example, if the dip is 30°, the distance will be reduced by 50%. The norminal distance from the contact, therefore, may be inappropriate for modeling cooling history. Contact aureoles can be ideal places to study the kinetics of metamorphic crystallization since modeling of cooling history can provide knowledge on the possible duration for metamorphic reactions. Although this was the impetus that initiated our CSD work in this area, we have not attempted thermal modeling due to the poor constraints on the geometry of the pluton-country rock contact.

The observed depletion of smaller crystals relative to larger crystals in the ln(n) vs. L diagrams (Fig. 4) may reflect two possibilities; (1) continuous growth and nucleation accompanied by Ostwald ripening (Marsh, 1988) or (2) changes in nucleation rate during metamorphism (Carlson, 1989). Ostwald ripening is a mean grain size increasing process due to the instabilities induced by surface energy, whereas changes in nucleation rate is caused by depletion of reactants. The changes in nucleation rate can modify the linear distribution because initially increasing but later decreasing nucleation rate may yield similar distribution curves in Fig. 4. Although it is difficult to identify the process (between Ostwald ripening and changes in nucleation rates) that caused the depletion in the smaller crystals, it is suggested that the observed depletion is at least partly due to Ostwald ripening, because the degree of the depletion is larger in the regions near the intrusion contact. Since Ostwald ripening is thermally-activated process (Joesten, 1991), the rate will be higher at high temperature conditions. From this viewpoint, following interpretation of Fig. 4 can be made. The left part of critical size in Fig. 4 show positive slope. Therefore, by equation 1 or 2, $G\tau<0$, and as a result of this inequality, crystals belong to size interval less than the critical size had experienced negative growth (dissolution of crystals). The positive slope for samples near intrusion contact (Fig. 4 a, b, c, and d) is steeper than that for samples away from intrusion contact. The trend may reveal more drastic ripening process near intrusion contact and this is consequence of temperature dependent nature of Ostwald ripening.

The overall difference in two groups may also be due to the differences in reactions involved in the formation of diopside. If diopside crystals of these two groups have been produced by different reactions during contact metamorphism, the observed trend may be due to different reaction rates. The wollastonite zone can be defined within 50m from the intrusion contact (Kim and Kim, 1996). Hence the samples near the intrusion contact belong to wollastonite zone while other samples belong to the diopside zone in the study area. There are two reactions including diopside as product phases (Kim and Kim, 1996);

$$3\ \text{calcite} + \text{tremolite} + 2\ \text{quartz} = 5\ \text{diopside} + H_2O + 3CO_2 \quad [R1]$$

$$6\ \text{calcite} + \text{K–feldspar} + 3\ \text{tremolite} = \text{phlogopite} + 12\ \text{diopside} + 2H_2O + 6CO_2 \quad [R2]$$

The reaction [R1] is most probable diopside-forming reaction in the diopside zone (Kim and Kim, 1996). In the wollastonite zone, some calcite pebbles are rimmed by phlogopite in the matrix around the rims consisting of diopside, suggesting [R2] in this zone (Kim and Kim, 1996). Consequently, diopside crystals in the two different zones might have been formed by different reactions and the resulting CSD may reflect the different reaction kinetics.

Conclusions

(1) In the ln(n) vs. L diagrams of diopside crystals, two different groups are recognized. The slopes of ln(n) vs. L diagrams for samples near the intrusion contact (distance from the contact less than 50 m) are gentler (1500 cm^{-1}) than those for samples away from intrusion contact (distance from the contact more than 100 m, 2500 cm^{-1}). This can be explained by the differences in growth rate and the time for crystallization or the differences in diopside-forming reactions.

(2) Depletion of small crystals decreases with increasing distance from the intrusion contact. The observed modification from the linear distribution may be due to the two processes, Ostwald ripening or changes of nucleation rate during metamorphism. Since the rate of Ostwald ripening is temperature-dependent, it is suggested that the observed depletion of small crystals is at least partly due to Ostwald ripening.

Acknowledgment

We wish to thank Dr. Youngdo Park (Korea University) for interest in this work and discussion, and Drs. Myungshik Jin (Korea Instute of Geology, Mining, and Materials), Changwhan Oh (Chunbuk University), and Moonsup Cho (Seoul National University), for their constructive comments. This work was supported by the fund from KOSEF (96-0703-07-01-3), and Korea University Academic Research Fund (1996).

References

Cashman, K.V., 1991, Textural constraints on the kinetics of crystallization of igneous rocks. Rev. Mineral., 24, 259-314.

Cashman, K.V., and Ferry, J., 1988, Crystal size distribution (CSD) in rocks and the kinetics and dynamics of crystallization III. Metamorphic crystallization. Contrib. Mineral. Petrol., 99, 401-415.

Cashman, K.V., and Marsh, B.D. 1988, Crystal size distributions (CSD) in igneous rocks and kinetics and dynamics of crystallization II. Macaopuhi lava lake Contrib. Mineral. Petrol., 99, 292-305.

Carlson, W.D., 1989, The significance of intergranular diffusion to the mechanism and kinetics of porphyroblast crystallization. Contrib. Mineral. Petrol., 103, 1-24.

Hong, S.S., 1985, A petrographic study on the contact metamorphism of the Ogcheon formation with Sogrisan granite in the southeastern Goesan area. MS thesis, Yonsei Univ.

Jin, M.S., Kim, S.J., Chi, S.J., S.C., Shin, and S.H., Choo, 1993, Radiometric ages of the Paleozoic and Mesozoic Granites in the middle part of the Ogcheon fold belt. KIGAM. Research Report.

Joesten, R., 1991, Kinetics of coarsening and diffusion-controlled mineral growth. Rev. Mineral., 26, 507-582.

Kim, S. and H.S. Kim, 1996, Fluid-rock interaction during contact metamorphism of the Hwanggangni Formation, Goesan, Korea, J. Petrol. Soc. Korea, 5, 21-34

Marsh, B.D., 1988, Crystal size distribution (CSD) in rocks and the kinetics and dynamics of crystallization. I. Theory. Contrib. Mineral. Petrol., 99, 277-291.

Randolph, A.D., and Larson, M.A., 1971, Theory of particulate processes. Academic press, New York, 251p.

Rasband, W., 1994, NIH Image, National Institute of Health, U.S.A

(1996년 11월 10일 접수)
(**책임편집 : 진명식**)

괴산지역 대야산 화강암체 주변 접촉변성대(황강리층)에서의 투휘석 결정 크기분포

김상명 · 김형식

고려대학교 이과대학 지구환경과학과

요 약 : 중생대 백악기에 관입한 대야산 화강암에 의해 열변성을 받은 황강리층에서는 투휘석 결정들이 나타난다. 이러한 투휘석 결정들의 크기분포는 열변성 작용이 진행되면서 연속적인 핵생성과 결정성장에 의해 형성되었음을 지시한다. 관입암체로 부터의 거리와 결정의 밀도-크기 그림에서의 기울기 간에 상관관계가 있음을 밝혔다. 경계부근부터의 거리가 50 m 내외인 경우 기울기는 1500 cm^{-1}로, 거리가 100 m 이상인 경우 기울기는 2500 cm^{-1}로 나타난다. 이러한 거리에 따른 기울기의 차이는 이 두 지역에서 결정성장률/결정성장시간의 차이 또는 투휘석을 형성하는 화학반응에 차이가 있었음을 지시한다. 로그결정밀도-크기 그림에서 작은 결정들은 상대적으로 적게 나타남이 관찰되며, 그 이유는 오스월드 숙성작용 또는 열변성 작용시 핵성장률의 감소일 가능성이 높다. 전술한 거리에 따른 기울기의 변화와 마찬가지로, 거리에 따른 작은 결정들의 고갈의 정도도 다르게 관찰된다. 이러한 고갈은 온도에 민감한 오스월드 숙성률에 따른 차이로 설명될 수 있다.

핵심어 : 결정크기분포, 투휘석, 핵 생성률, 결정 성장률, 오스월드 숙성률